

This article was downloaded by: [NIST National Institutes of Standards &]

On: 01 August 2011, At: 06:36

Publisher: Taylor & Francis

Informa Ltd Registered in England and Wales Registered Number: 1072954 Registered office: Mortimer House, 37-41 Mortimer Street, London W1T 3JH, UK



## Aerosol Science and Technology

Publication details, including instructions for authors and subscription information:

<http://www.tandfonline.com/loi/uast20>

### Quantification and Compensation of Nonspecific Analyte Aggregation in Electrospray Sampling

Mingdong Li<sup>a b</sup>, Suvajyoti Guha<sup>a b</sup>, Rebecca Zangmeister<sup>b</sup>, Michael J. Tarlov<sup>b</sup> & Michael R. Zachariah<sup>a b</sup>

<sup>a</sup> Departments of Mechanical Engineering and Chemistry and Biochemistry, University of Maryland, College Park, Maryland, USA

<sup>b</sup> Process Measurements Division, National Institute of Standards and Technology, Gaithersburg, Maryland, USA

Available online: 30 Mar 2011

To cite this article: Mingdong Li, Suvajyoti Guha, Rebecca Zangmeister, Michael J. Tarlov & Michael R. Zachariah (2011): Quantification and Compensation of Nonspecific Analyte Aggregation in Electrospray Sampling, *Aerosol Science and Technology*, 45:7, 849-860

To link to this article: <http://dx.doi.org/10.1080/02786826.2011.566901>

PLEASE SCROLL DOWN FOR ARTICLE

Full terms and conditions of use: <http://www.tandfonline.com/page/terms-and-conditions>

This article may be used for research, teaching and private study purposes. Any substantial or systematic reproduction, re-distribution, re-selling, loan, sub-licensing, systematic supply or distribution in any form to anyone is expressly forbidden.

The publisher does not give any warranty express or implied or make any representation that the contents will be complete or accurate or up to date. The accuracy of any instructions, formulae and drug doses should be independently verified with primary sources. The publisher shall not be liable for any loss, actions, claims, proceedings, demand or costs or damages whatsoever or howsoever caused arising directly or indirectly in connection with or arising out of the use of this material.



# Quantification and Compensation of Nonspecific Analyte Aggregation in Electrospray Sampling

Mingdong Li,<sup>1,2</sup> Suvajyoti Guha,<sup>1,2</sup> Rebecca Zangmeister,<sup>2</sup> Michael J. Tarlov,<sup>2</sup> and Michael R. Zachariah<sup>1,2</sup>

<sup>1</sup>*Departments of Mechanical Engineering and Chemistry and Biochemistry, University of Maryland, College Park, Maryland, USA*

<sup>2</sup>*Process Measurements Division, National Institute of Standards and Technology, Gaithersburg, Maryland, USA*

---

Electrospray (ES) sources are commonly used to introduce non-volatile materials (e.g., nanoparticles, proteins, etc.) to the gas phase for characterization by mass spectrometry or ion mobility. Recent studies in our group using ES ion mobility to characterize protein aggregation in solution have raised the question as to whether the ES itself induces aggregation and thus corrupts the results. In this article, we develop a statistical model to determine the extent to which the ES process induces the formation of dimers and higher-order aggregates. The model is validated through ES differential mobility experiments using gold nanoparticles. The results show that the extent of droplet-induced aggregation is quite severe and previously reported cutoff criterion is inadequate. We use the model in conjunction with experiment to show the true dimer concentration in a protein solution as a function of concentration. The model is extendable to any ES source analytical system and to higher aggregation states. For users only interested in implementation of the theory, we provide a section that summarizes the relevant formulas.

---

[Supplementary materials are available for this article. Go to the publisher's online edition of *Aerosol Science and Technology* to view the free supplementary files.]

## 1. INTRODUCTION

Protein aggregation is a major concern with nearly all protein therapeutics because of their potential for immunogenicity

---

Received 22 November 2010; accepted 8 February 2011.

The authors thank Dr. Joshua Wayment for providing us Rmab samples and Dr. James Falabella for providing us data from his analytical ultracentrifuge measurements of Rmab. Commercial equipment, instruments, or materials identified in this report does not imply recommendation or endorsement by the University of Maryland or the National Institute of Standards and Technology.

Address correspondence to Michael R. Zachariah, Department of Mechanical Engineering, University of Maryland, 2125 Martin Hall, College Park, MD 20742, USA. E-mail: mrz@umd.edu

in patients. One of the tools we investigate to measure protein aggregation involves using electrospray (ES) to generate vapor-phase dispersed material. These vapor-phase dispersed materials can then be analyzed by ion mobility methods named differential mobility analyzer (DMA), also known as gas-phase electrophoretic molecular analysis (GEMMA; Kaufman et al. 1996; Bacher et al. 2001; Kim and Zachariah 2005, 2006, 2007; Pease et al. 2008) or mass spectrometry (MS; Light-Wahl et al. 1993, 1994; Ayed et al. 1998; Nettleton et al. 2000; Lane et al. 2009) methods. These techniques have the potential to characterize the distribution of oligomeric protein species in solution.

To accurately characterize protein oligomers in solution, the ES process should be thoroughly understood in order to correct for any potential bias originating from droplet formation. The mechanism of ES has been treated in great detail by Kebarle and Tang (1993) and Gaskell (1997). In ES, the application of a high voltage to a capillary can induce, due to columbic repulsion, small droplet formation. These droplets undergo evaporation coupled with collisions, as well as fissions when reaching their Rayleigh limits. There are two major theories employed to explain the ES process to eventually produce gas-phase analyte ions: charge residue model (CRM; Dole et al. 1968) and ion evaporation model (IEM; Iribarne and Thomson 1976; Kebarle 2000). In the IEM, it is thought that the strong E-field at the drop surface results in ion emission at a critical drop radius. CRM suggests that droplets undergo a series of fissions to a final drop size where subsequent solvent evaporation leaves behind the residue analyte (e.g., protein, particle, virus, etc.). It is well accepted that large and compact multiply charged ions, such as globular proteins, which are the analytes of interest in this work, are produced as charged residues after complete drop evaporation by CRM (Fernandez de la Mora 2000; Gamero-Castano and Fernandez de la Mora 2000a, 2000b; Ku and Fernandez de la Mora 2004; Hogan et al. 2009). In this study, we will not concern ourselves as to the detail fission process of CRM, as we

will bypass the nature of the ES process by directly measuring the final droplet size distribution.

As mentioned, one of the potential uses of ES-DMA or ES-MS is to study oligomerization in solution. For this application, one must consider whether the measured oligomer distribution reflects the actual distribution in the sample, or if the observed oligomers are an artifact of the ES process. For example, one potential concern is where two or more analyte molecules or particles occupy a volume encompassing what becomes a final electrosprayed droplet. This scenario would result in the observation of oligomers that originated from the droplet formation process.

The usual procedure in the use of a DMA is to charge neutralize the droplets with a bipolar ion source (e.g., Po-210), to yield a bipolar equilibrium charge distribution (Wiedensohler 1988; Chen et al. 1995). The neutralizer stops the fission process at an early stage leading to larger final droplet sizes. In such a situation, the CRM is expected to hold and solvent evaporation could lead to unintentional analyte oligomers. Lenggoro et al. (2002) and Pease et al. (2008) have presented a method to provide an upper workable concentration to mitigate this problem. Kaufman et al. (1996) have also described a simple criterion to determine whether there are intrinsic dimers in solution based on DMA size distributions by assuming that all droplets were of the same size. However, that criterion cannot quantify the intrinsic aggregates in solution. The unintentional (nonspecific) analyte aggregation may also be a problem in ES without a neutralizer. While the final droplet size is much smaller because of a series of fissions, the net effect is the same. Lane et al. (2009) addressed the same nonspecific analyte aggregation problem as in our work, in an ES-MS without a neutralizer, and developed a Monte Carlo approach for assessing the specificity of protein oligomers observed in ES mass spectra. However, because they did not have a direct measure of the drop size, they assumed that all droplets were of the same size and the droplet size was selected to fit the experimental data best. They simulated a Poisson distribution, which was also employed by Lewis et al. (1994) and Kaufman et al. (1996). Hogan and Biswas (2008a) developed two Monte-Carlo-based models to predict the efficiency of ES ionization for macromolecules and to study the porous film deposition by electrohydrodynamic atomization of nanoparticle sols (Hogan and Biswas 2008b). In their Monte-Carlo-based models, the size distributions of sprayed particles are determined by the convolution of a Poisson distribution within the initial droplet size distribution and the initial ES droplet size distribution is represented by a lognormal distribution function. Although a lognormal distribution may be a good representation for the initial droplet size distribution of ES in theoretical calculation and simulation, the final droplet size distribution of ES can be obtained directly from experiments (Section 3.4) and is not necessarily an exact lognormal distribution (Figures 2a, b, and 6).

All the studies above did not consider a joint Poisson distribution and so cannot quantify the intrinsic aggregates in solution correctly. Monte Carlo approaches cannot provide an explicit

analytical expression to calculate the nonspecific aggregation and characterize the true oligomerization in solution.

This article focuses on developing an experimentally verified theory that will enable one to distinguish ES-induced aggregates from the intrinsic aggregates, and without the need to model the details of the ES fission process, through a direct measure of the final droplet size distribution. We demonstrate our theory on our own ES-DMA work. The approach is generic to any ES process and thus can be applied equally to either ion mobility or mass spectrometry analysis. For users only interested in the implementation of the theory, we provide a section that summarizes the relevant formulas (Section 5).

## 2. THEORY

### 2.1. Physical Aggregation (Droplet-Induced Aggregation) of Identical Particles

Because the spatial distribution of analytes in solution is statistical, our theoretical treatment was developed by probabilistic analysis. If a final droplet generated in ES is a random sample of the solution, and the particles in the solution are identical and independent, the probability of  $k$  particles in a given droplet obeys a Poisson distribution (Lewis et al. 1994; Kaufman et al. 1996; Edd et al. 2008; Abate et al. 2009) and is given by

$$Q(k, \lambda) = \frac{e^{-\lambda} \lambda^k}{k!}, \quad [1]$$

where  $\lambda$  is the mean number of particles per droplet and is given by

$$\lambda = V_d C_p = \frac{1}{6} \pi D_d^3 C_p, \quad [2]$$

where  $V_d$  is the droplet volume,  $D_d$  is the droplet diameter, and  $C_p$  is the number concentration of the particles in solution (the number of particles per volume).

Lewis et al. (1994) and Kaufman et al. (1996) asserted that the probability to find a certain number of particles in a single droplet follows a Poisson distribution, but did not provide a justification. We use a statistical model to mathematically justify that the particles indeed follow a Poisson distribution in solution. This model is discussed in greater detail in the online supplemental information.

Consider a solution containing an analyte (particles). In the period of time that one unit volume of solution is sprayed,  $1/V_d$  droplets are generated, and the total number of particles passing through the capillary and thus incorporated within the droplets is  $C_p$ . If we define one event as one particle being encapsulated in a droplet and assign  $\Delta t$  as the average time to generate one droplet, then the rate of this event occurring is  $R = C_p/(\Delta t \times 1/V_d) = V_d C_p/\Delta t$ . The expected number of occurrences in this interval  $\Delta t$  is  $\lambda = R\Delta t = V_d C_p$ . The probability that there are exactly  $k$  occurrences in this interval is given by a Poisson distribution,  $Q(k, \lambda)$ , with parameter  $\lambda$ . Further justification on the

use of a Poisson distribution is provided in online supplemental information A.

Assuming a monomodal droplet size distribution  $f(D_d)$ , the average value of the Poisson distribution parameter  $\lambda$  is given by

$$\bar{\lambda} = \sum_i f(D_{d,i})\lambda = C_p \sum_i \frac{1}{6}\pi D_{d,i}^3 f(D_{d,i}) = C_p \bar{V}_d, \quad [3]$$

where

$$\bar{V}_d = \sum_i \frac{1}{6}\pi D_{d,i}^3 f(D_{d,i}), \quad [4]$$

is the average droplet volume,

$$\sum_i f(D_{d,i}) = 1.$$

The discussion about droplet size measurement is addressed in Section 3.4.

Then the probability of droplet-induced aggregation follows:

$$Q(k, \bar{\lambda}) = \frac{e^{-\bar{\lambda}} \bar{\lambda}^k}{k!}. \quad [5]$$

where  $k$  is the order of aggregation.

If the solution contains only monomers, then based on Equation (5), the droplet-induced dimer to monomer ratio is

$$\frac{Q(2, \bar{\lambda})}{Q(1, \bar{\lambda})} = \frac{\bar{\lambda}}{2}. \quad [6]$$

In this scenario, there are no intrinsic dimers in solution. Therefore, the observed dimer to monomer ratio is the same as the induced ratio.

Equation (6) is useful because it provides a convenient criterion to determine if there are any intrinsic dimers in the solution. Simply, if the observed dimers are higher than that computed by Equation (6), we can ascribe the difference to the intrinsic dimers in the solution. This point has also been partially addressed by Kaufman et al. (1996), but they assumed that all droplets were of the same size.

## 2.2. Quantitative Determination of Intrinsic Aggregates in Solution

The ‘‘dimer-to-monomer ratio’’ criterion, as demonstrated above, is valid if there are few to no dimers existing in the solution, but it fails where the intrinsic oligomers such as dimers, trimers, etc., have a substantial contribution to the total particle concentration, as is common for solutions containing protein oligomers. In this section, we present a strategy to quantify the aggregate ratio of intrinsic dimers to intrinsic monomers in solution for an arbitrary condition. This same strategy can also be expanded to quantify any higher-order aggregates. Be-

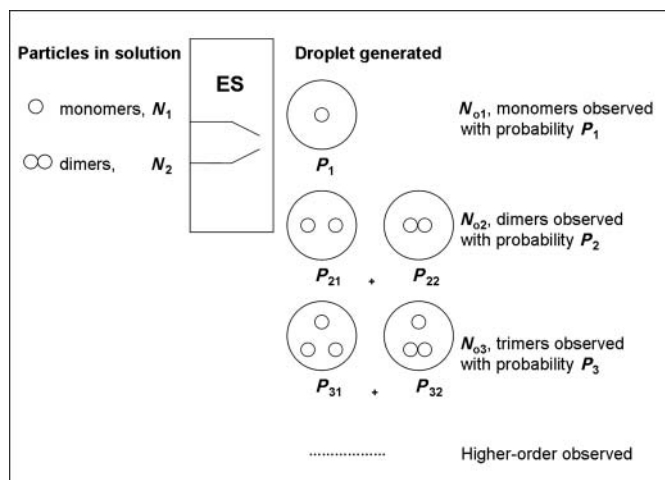


FIG. 1. Physical representation of the probability distribution of induced and intrinsic aggregate distributions from ES.

fore addressing the mathematics of the process, we consider the physical constructs of the problem.

A schematic description of how intrinsic and induced oligomers may be distributed within ES droplets is shown in Figure 1. Consider there are  $N_1$  monomers and  $N_2$  dimers in solution. Following ES,  $N_{o1}$  monomers,  $N_{o2}$  dimers, and  $N_{o3}$  trimers are observed with probabilities  $P_1$ ,  $P_2$ , and  $P_3$ . There is only one possible condition for the observation of monomers; that is, only one monomer in a single droplet generated by ES has a probability of  $P_1$ . For the observed dimers, there are two possibilities. One is that two monomers are captured within a single droplet with probability  $P_{21}$ , creating an induced dimer, and the other possibility is that there is one intrinsic dimer in a single droplet with probability  $P_{22}$ . Similarly for trimers, there are two situations: three monomers captured into a droplet with probability  $P_{31}$  or one monomer and one dimer captured within the same droplet with probability  $P_{32}$ . With this construct, we can obtain the following two relationships:

$$\frac{N_{o2}}{N_{o1}} = \frac{P_2}{P_1} = \frac{P_{21} + P_{22}}{P_1}, \quad [7]$$

$$\frac{N_{o3}}{N_{o1}} = \frac{P_3}{P_1} = \frac{P_{31} + P_{32}}{P_1}. \quad [8]$$

Assuming the spatial distribution of monomers is random, the number of monomers in a droplet should follow a Poisson distribution with parameter  $\lambda_1$ :

$$Q(k, \lambda_1) = \frac{e^{-\lambda_1} \lambda_1^k}{k!}, \quad [9]$$

where

$$\lambda_1 = V_d C_{p1} = \frac{1}{6}\pi D_d^3 C_{p1}. \quad [10]$$

Here,  $C_{p1}$  the number concentration of monomers in solution,  $V_d$  is the droplet volume, and  $D_d$  is the droplet diameter.

The number of dimers in a droplet follows a Poisson distribution with parameter  $\lambda_2$ :

$$Q(k, \lambda_2) = \frac{e^{-\lambda_2} \lambda_2^k}{k!}, \quad [11]$$

$$\lambda_2 = V_d C_{p2} = \frac{1}{6} \pi D_d^3 C_{p2}, \quad [12]$$

where  $C_{p2}$  is the number concentration of dimers in solution.

Assuming the two Poisson distributions are independent, so

$$P_1 = Q(1, \lambda_1) Q(0, \lambda_2) = e^{-(\lambda_1 + \lambda_2)} \lambda_1, \quad [13]$$

$$P_{21} = Q(2, \lambda_1) Q(0, \lambda_2) = e^{-(\lambda_1 + \lambda_2)} \frac{\lambda_1^2}{2}, \quad [14]$$

$$P_{22} = Q(0, \lambda_1) Q(1, \lambda_2) = e^{-(\lambda_1 + \lambda_2)} \lambda_2, \quad [15]$$

$$P_{31} = Q(3, \lambda_1) Q(0, \lambda_2) = e^{-(\lambda_1 + \lambda_2)} \frac{\lambda_1^3}{6}, \quad [16]$$

$$P_{32} = Q(1, \lambda_1) Q(1, \lambda_2) = e^{-(\lambda_1 + \lambda_2)} \lambda_1 \lambda_2. \quad [17]$$

Equations (13)–(17) were obtained assuming that oligomers in the ES process follow an independent joint Poisson distribution. An accurate form of  $(P_1, P_2)$  can be obtained using the methodology described in the online supplemental information A. We use Equations (13)–(17) here for the calculations in this work.

Using relations (13)–(17), (7), and (8), we get the following equation set for a single droplet size:

$$\frac{N_{o2}}{N_{o1}} = \frac{P_2}{P_1}, \quad [18]$$

$$\frac{N_{o3}}{N_{o1}} = \frac{P_3}{P_1}, \quad [19]$$

$$P_1 = e^{-(\lambda_1 + \lambda_2)} \lambda_1, \quad [20]$$

$$P_2 = e^{-(\lambda_1 + \lambda_2)} \left( \frac{\lambda_1^2}{2} + \lambda_2 \right), \quad [21]$$

$$P_3 = e^{-(\lambda_1 + \lambda_2)} \left( \frac{\lambda_1^3}{6} + \lambda_1 \lambda_2 \right), \quad [22]$$

where

$$\lambda_1 = V_d C_{p1} \quad [23]$$

$$\lambda_2 = V_d C_{p2}. \quad [24]$$

If we consider the droplet size distribution from an ES source,  $f(D_d)$ , a general relationship for the dimer to monomer ratio and the trimer to monomer ratio is (proof is provided in the online

supplemental information B)

$$\frac{N_{o2}}{N_{o1}} = \frac{\int f(D_d) P_2 dD_d}{\int f(D_d) P_1 dD_d}, \quad [25]$$

$$\frac{N_{o3}}{N_{o1}} = \frac{\int f(D_d) P_3 dD_d}{\int f(D_d) P_1 dD_d}, \quad [26]$$

where  $\int f(D_d) dD_d = 1$ .

An inversion procedure could be developed for intrinsic concentrations,  $C_{p1}$  and  $C_{p2}$ , based on Equations (25) and (26). Although it is difficult to solve Equations (25) and (26) for analytical expressions of  $C_{p1}$  and  $C_{p2}$  directly, accurate approximations can be obtained under some limiting conditions.

### 2.3. Limiting Cases

In this work, we consider two simple cases: monomodal and bimodal droplet size distributions.

#### 2.3.1. Monomodal and Narrow Droplet Size Distribution $f(D_d)$

If the droplet size distribution  $f(D_d)$  can be considered to be monomodal and relatively narrow, as, for example, we show in Figure 2a, a droplet size distribution from ES measured at 20 mmol/L ammonium acetate in sucrose based on Section 3.4. Equations (25) and (26) can be evaluated with one average droplet volume:

$$\frac{N_{o2}}{N_{o1}} \approx \frac{P_2|_{V_d=\bar{V}_d}}{P_1|_{V_d=\bar{V}_d}} = \frac{\bar{V}_d C_{p1}}{2} + \frac{C_{p2}}{C_{p1}}, \quad [27]$$

$$\frac{N_{o3}}{N_{o1}} \approx \frac{P_3|_{V_d=\bar{V}_d}}{P_1|_{V_d=\bar{V}_d}} = \frac{\bar{V}_d^2 C_{p1}^2}{6} + \bar{V}_d C_{p2}, \quad [28]$$

where

$$\bar{V}_d = \sum_i f(D_{d,i}) V_{d,i} = \sum_i f(D_{d,i}) \frac{1}{6} \pi D_{d,i}^3 \quad [29]$$

is the average droplet volume,

$$\sum_i f(D_{d,i}) = 1,$$

$N_{o2}$  is the observed number of monomers after ES,  $N_{o1}$  is the observed number of dimers after ES.

The monomodal approximation above can be improved by using three average droplet volumes in three regions (peak left, main peak, and peak right) in Figure 3 and solving Equations (25) and (26).

#### 2.3.2. Bimodal Droplet Size Distribution $f(D_d)$

If the droplet size distribution  $f(D_d)$  is bimodal, as, for example, shown in Figure 2b, and  $\bar{V}_{d2}(C_{p1} + C_{p2})$  is not much

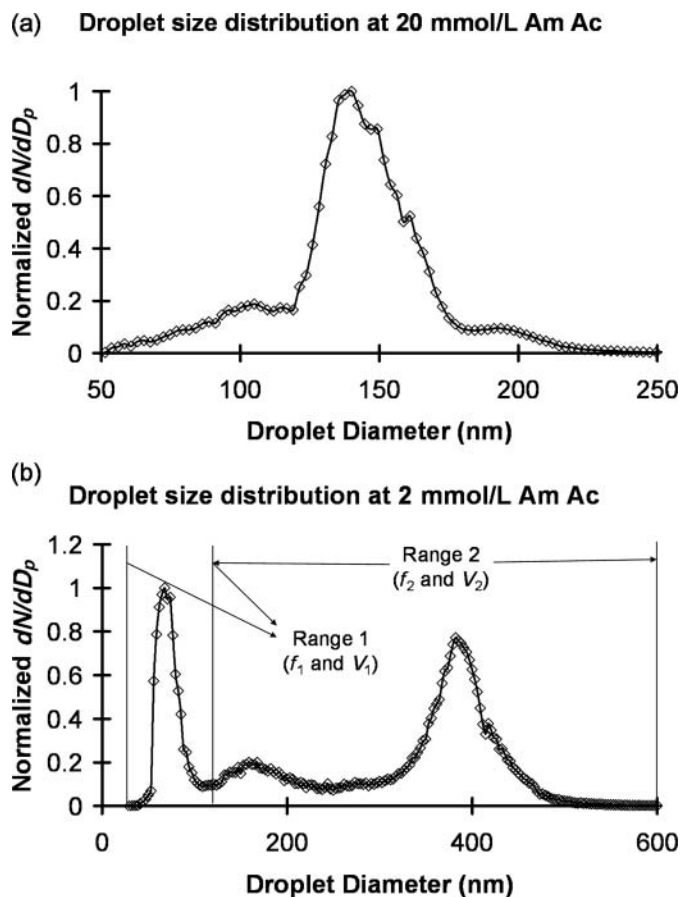


FIG. 2. (a) ES monomodal and narrow droplet size distribution [20 mmol ammonium acetate (Am Ac) with the chamber pressure in ES at PSI 3.7 ( $2.55 \times 10^4$  Pa) and a carrier gas in ES of 1 L/min purified air and 0.2 L/min carbon dioxide] for Rituxan samples in Sections 4.1.1 and 4.2. (b) ES droplet with a bimodal size distribution (2 mmol ammonium acetate (Am Ac) with the chamber pressure in ES at PSI 3.7 ( $2.55 \times 10^4$  Pa) and a carrier gas in ES of 1 L/min purified air and 0.2 L/min carbon dioxide) for Au-NPs Samples 1 and 2 in Section 4.3.

greater than unity, then Equation (25) can be approximated by using two average droplet volumes. (The detailed derivations and discussions are given in a separate manuscript.)

$$\frac{N_{o2}}{N_{o1}} \approx \frac{f_1 P_2|_{V_d=\bar{V}_{d1}} + f_2 P_2|_{V_d=\bar{V}_{d2}}}{f_1 P_1|_{V_d=\bar{V}_{d1}} + f_2 P_1|_{V_d=\bar{V}_{d2}}} \approx \frac{\bar{V}_{d2} C_{p1}}{2} + \frac{C_{p2}}{C_{p1}}, \quad [30]$$

where

$$\sum_i f(D_{d,i}) = 1, \quad [31]$$

$$f_1 = \sum_i^{range1} f(D_{d,i}), \quad [32]$$

$$f_2 = \sum_i^{range2} f(D_{d,i}),$$

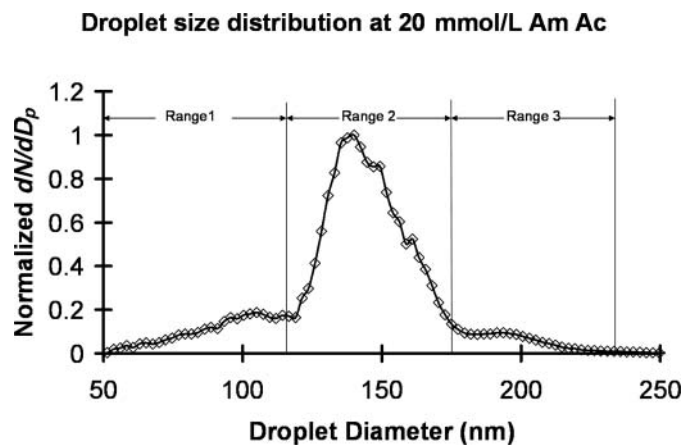


FIG. 3. ES monomodal and narrow droplet size distribution (20 mmol ammonium acetate (Am Ac) with the chamber pressure in ES at PSI 3.7 ( $2.55 \times 10^4$  Pa) and a carrier gas in ES of 1 L/min purified air and 0.2 L/min carbon dioxide). The monomodal approximation can be improved by using three average droplet volumes in three regions and solving Equations (25) and (26).

$$\bar{V}_{d1} = \frac{1}{f_1} \sum_i^{range1} f(D_{d,i}) V_{d,i} = \frac{1}{f_1} \sum_i^{range1} f(D_{d,i}) \frac{1}{6} \pi D_{d,i}^3, \quad [33]$$

$$\bar{V}_{d2} = \frac{1}{f_2} \sum_i^{range2} f(D_{d,i}) V_{d,i} = \frac{1}{f_2} \sum_i^{range2} f(D_{d,i}) \frac{1}{6} \pi D_{d,i}^3, \quad [34]$$

where  $f_1$  is the fraction of the droplets with the sizes within range 1 including the first size mode,  $f_2$  is the fraction of the droplets with the sizes within range 2 including the second mode,  $\bar{V}_{d1}$  is the average droplet volume within range 1, and  $\bar{V}_{d2}$  is the average droplet volume within range 2.

The end result of this analysis shows that using experimental observation of the observed monomers, dimers, and trimers ( $N_{o1}$ ,  $N_{o2}$ ,  $N_{o3}$ ), one can use relations (27) and (28) to obtain the concentration of intrinsic monomers and dimers ( $C_{p1}$ ,  $C_{p2}$ ) for a monodispersed droplet size distribution and under the appropriate conditions described above, use relation (30) for a bimodal droplet size distribution. For a general droplet size distribution, Equations (25) and (26) should be used.

### 3. MATERIALS AND METHODS

We demonstrate our model by examining gold nanoparticles (Au-NPs) with an ES-neutralizer-DMA-condensation particle counter (ES-neutralizer-DMA-CPC) system described previously (Tsai et al. 2008). In order to show the efficacy of this technique, highly concentrated Au-NPs and large volume droplets in ES are needed. ES of highly concentrated Au-NPs is challenging because of the instability of the capillary that arises from the highly concentrated Au-NPs under low ionic strength

and the presence of solution stabilizing citrate salts, which can result in the formation of nonvolatile particles that interfere with the DMA measurement (Tsai et al. 2008). The protocol for obtaining high concentrations of Au-NPs is given below and large droplet sizes can be obtained by using low conductivity solutions along with large capillary diameters for the ES.

Finally, we use a Rituxan monoclonal antibody (Rmab) to show the application of our approach to quantify protein aggregate distributions in solution.

### 3.1. Au-NP Preparation

Commercially available citrate-stabilized monodisperse Au colloids (10 nm,  $5.7 \times 10^{12}$  particles/mL, Ted Pella, Inc.) were used. A 1.5 mL solution of the as-received Au colloids was centrifuged at 13,200 rpm for 45 min, and 1.46–1.47 mL of the supernatant was removed and replaced with an equivalent volume of aqueous 2 mmol/L ammonium acetate solution at pH 10. This step was performed to remove most of the citrate stabilizer, which would otherwise coat the Au-NPs upon ES. The pH of the ammonium acetate solution was adjusted by the addition of ammonium hydroxide. Then, the solution was centrifuged at 13,200 rpm again for 15 min and 1.4 mL of supernatant was removed to obtain a highly concentrated Au-NP sample that was then electrosprayed into the DMA-CPC system. At these high concentrations, the oligomer peaks were not resolved (data not shown), and hence, these samples were diluted 2 $\times$ , 4 $\times$ , and 8 $\times$ , for the ES studies.

### 3.2. Rmab Solution Preparation

Formulated Rmab was purified using a protein A affinity column. Purified Rmab was stored at  $-18^\circ\text{C}$  in 25 mmol/L Tris buffer, pH 7.4, with 0.01%  $\text{NaN}_3$  added as a preservative. Immediately prior to use in ES studies, the storage buffer was exchanged for 20 mmol/L ammonium acetate, pH 7, by washing all salts from Rmab using a centrifugal filter device with a weight cutoff of 30 kDa. The concentration of Rmab in 20 mmol/L ammonium acetate was adjusted to 1 mg/mL as verified by measuring the maximum absorbance at 280 nm and using a molar absorptivity of  $236,020 (\text{mol/L})^{-1} \text{cm}^{-1}$ . Working solutions of concentrations 100, 50, 25, 10, and 5  $\mu\text{g/mL}$  were made by dilution and used for ES studies.

### 3.3. Particle Measurements

Aerosolized droplets were generated using a 40- $\mu\text{m}$  inner diameter capillary for Au-NP samples and a 25- $\mu\text{m}$  inner diameter capillary for Rmab mounted in an electrospray aerosol generator (Model 3480, TSI, Inc.), and the liquid flow rates through the capillaries were 433 and 66 nL/min, respectively (TSI Model 3480 Electrospray Aerosol Generator Menu). The ES was operated with a carrier gas of 1 L/min purified air and 0.2 L/min carbon dioxide. The aerosolized droplets were passed through a neutralizer and entered a DMA (Model 3485 Nano DMA column, TSI, Inc.) for particle size measurement, and were counted with an ultrafine CPC (Model 3025A, TSI, Inc.).

More details on the measurement method can be found in Tsai et al. (2008).

### 3.4. Droplet Size Measurements

The use of relations (3) or (4) and (31)–(34) requires knowledge of the droplet size. Droplet size was determined by electrospraying a known concentration of sucrose solution and measuring the resultant dry particle size. The sucrose solution (1.26% v/v) was prepared and diluted into 20 mmol/L ammonium acetate buffer, pH 7, giving a final concentration of 0.063% v/v. The ES droplet size of this solution was evaluated by (Chen et al. 1995)

$$D_d = \frac{1}{C_s^{1/3}} D_s, \quad [35]$$

where  $D_d$  is the droplet diameter,  $D_s$  is the sucrose particle diameter after drying, and  $C_s$  is the sucrose volume/volume concentration.

Note that an alternative approach discussed in the next section that involves measurement of a series dilutions of the original analyte mitigates the need to know the drop size distribution.

## 4. RESULTS AND DISCUSSION

### 4.1. Evidence of Droplet-Induced Aggregation

To illustrate the magnitude of the problem and the errors that can occur if the droplet-induced effects are not accounted for, we consider three examples. The first is a study to characterize the oligomers of Rmab at different concentrations (Section 4.1.1), and the second where an Rmab sample at the concentration of 100  $\mu\text{g/mL}$  was measured under different ES droplet volumes by varying the ES chamber pressure (Section 4.1.2). Both experiments were operated by our ES-Neutralizer-DMA-CPC. The third is shown in Section 4.2 by comparing our ES-Neutralizer-DMA-CPC results with analytical ultracentrifuge (Ebel 2004; Howlett et al. 2006) measurements directly on the solution, under the same conditions.

#### 4.1.1. Effect of Concentration

First, the sucrose size distributions in the 20 mmol/L ammonium acetate buffer at pH 7 were obtained that provide us with the droplet size distributions for Rituxan using Equation (35). Figure 2 shows the droplet size distributions at pH 7 in 20 mmol/L ammonium acetate buffer of Rituxan at concentrations of 5, 10, 25, 50, and 100  $\mu\text{g/mL}$ . On the basis of the distribution in Figure 2a and Equation (4), the average droplet volume was calculated to be  $1.64 \times 10^{-21} \text{m}^3$ . The average droplet size is 141 nm, which is in reasonable agreement with previous results (Kaufman 2000; Lenggono et al. 2002; Pease et al. 2008). According to Pease et al. (2008), the corresponding “cutoff” concentration at which the observed aggregates are intrinsic to the sample is 169  $\mu\text{g/mL}$ .

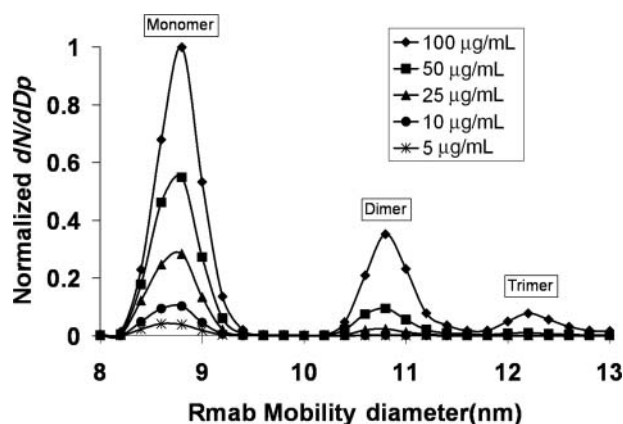


FIG. 4. The observed ES-DMA size distributions of Rituxan concentration at  $5 \mu\text{g/mL}$  (stars),  $10 \mu\text{g/mL}$  (circles),  $25 \mu\text{g/mL}$  (triangles),  $50 \mu\text{g/mL}$  (squares), and  $100 \mu\text{g/mL}$  (rhombuses) at pH 7 in 20 mmol/L ammonium acetate buffer with the chamber pressure in ES at PSI 3.7 ( $2.55 \times 10^4 \text{ Pa}$ ).

Figure 4 shows observed ES-DMA size distributions of Rituxan concentrations at 5, 10, 25, 50, and  $100 \mu\text{g/mL}$  with the chamber pressure in ES at PSI 3.7 ( $2.55 \times 10^4 \text{ Pa}$ ). A large proportion of oligomers are observed in these measurements.

The ratios of the number of observed dimer to the monomer against the Rituxan concentrations at 5, 10, 25, 50, and  $100 \mu\text{g/mL}$  are plotted in Figure 5 (rhombuses). On the basis of the droplet-induced dimer to monomer ratio of identical particles following Equation (6), we obtain a second curve at the same concentrations in Figure 5 (line with filled squares). The curve deduced from the droplet-induced model lies slightly below the data points indicating that most dimers observed in Figures 4 and 5 by ES-DMA are droplet induced and that the cut-off ( $169 \mu\text{g/mL}$ ) criterion as used by Lenggoro et al. (2002) and Pease et al. (2008) significantly underpredicts the extent of the problem and is insufficient in eliminating droplet-induced aggregation effects. Hence, we conclude that induced aggregation is a problem at all concentrations and the approach described

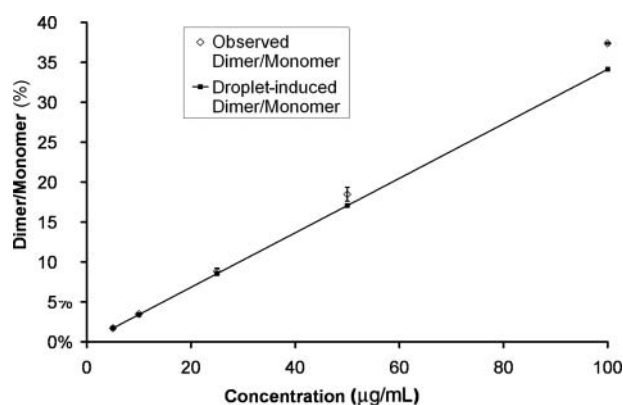


FIG. 5. The ratios of dimer to the total number of dimer and monomers at pH 7 observed by ES-DMA as a function of Rituxan concentration at 5, 10, 25, 50, and  $100 \mu\text{g/mL}$  (rhombuses). Ratios from droplet-induced dimers (line with filled squares) at the same concentrations calculated based on Equation (6).

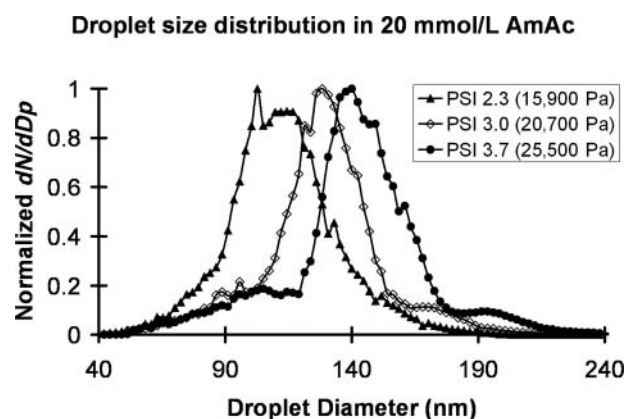


FIG. 6. ES droplet size distributions at pH 7 in 20 mmol/L ammonium acetate (Am Ac) buffer. The triangle, rhombus, and circle distributions are those of the same sample with the chamber pressure in ES at 2.3 PSI ( $1.59 \times 10^4 \text{ Pa}$ ), 3.0 PSI ( $2.07 \times 10^4 \text{ Pa}$ ), and 3.7 PSI ( $2.55 \times 10^4 \text{ Pa}$ ), respectively.

above should be used to determine the extent of physical aggregation.

To a first approximation, the difference between the experimental data and the induced dimer curve can provide the true dimer concentration. A more rigorous approach is to include the effect of intrinsic dimer present in the sample. When the intrinsic dimer is present, the concentration of monomer is lower, and thus, the induced dimer fraction will also be lower. This issue could be solved using an iterative procedure; however, we described a simpler approach below.

#### 4.1.2. Effect of Droplet Volume

In order to make it clearer that the observed dimers in our ES-DMA measurements of Rituxan at the concentration of  $100 \mu\text{g/mL}$  are not fully intrinsic in solution but mostly droplet induced, we changed the ES droplet volumes by varying the ES chamber pressure (Figure 6). If the observed dimers are intrinsic, the ratio of observed dimer to monomer should not change when varying the droplet size, but if a substantial part of the observed dimers is droplet induced, varying the droplet size would change the ratio based on Equation (27). In Table 1, the results show that the observed dimer to monomer ratio changes from 20.6% to 29.5%, then to 37.4% for one capillary, and from 23% to 31%, then to 41% for another capillary when varying the ES chamber pressure from PSI 2.3 ( $1.59 \times 10^4 \text{ Pa}$ ) to PSI 3.0 ( $2.07 \times 10^4 \text{ Pa}$ ) and then to PSI 3.7 ( $2.55 \times 10^4 \text{ Pa}$ ). This shows clearly that the observed dimers cannot be fully intrinsic. Also, after correction for droplet-induced dimers based on our model (the strategy in Section 4.2), the intrinsic dimer to monomer ratios goes to 5.4%, 7.5%, and 7.8% for the first capillary, and for 4%, 4.7%, and 7.3% for the second capillary. The average values for the two experiments are 4.7%, 6.1%, and 7.6% with the chamber pressure in ES at 2.3 PSI ( $1.59 \times 10^4 \text{ Pa}$ ), 3.0 PSI ( $2.07 \times 10^4 \text{ Pa}$ ), and 3.7 PSI ( $2.55 \times 10^4 \text{ Pa}$ ), respectively, which are reasonably consistent with the analytical ultracentrifuge (Ebel 2004; Howlett et al. 2006) measurements directly on the

TABLE 1

The ratios of observed dimers to monomers from DMA measurement by varying the ES droplet volumes, and the ratios of dimers to monomers after correction for drop-induced dimers based on our model (the strategy in Section 4.2) for Rituxan at the concentration of 100  $\mu\text{g/mL}$  at pH 7 in 20 mmol/L ammonium acetate buffer

	ES chamber pressure (Pa)	Average final droplet volume ( $\text{m}^3$ )	Observed dimer to monomer ratio (%)	Dimer to monomer ratio after correction for drop-induced dimers (%)
Capillary 1	PSI2.3 ( $1.59 \times 10^4$ )	8.15E-22	20.6	5.4
	PSI3.0 ( $2.07 \times 10^4$ )	1.22E-21	29.5	7.5
	PSI3.7 ( $2.55 \times 10^4$ )	1.64E-21	37.4	7.8
Capillary 2	PSI2.3 ( $1.59 \times 10^4$ )	9.91E-22	23.1	4.0
	PSI3.0 ( $2.07 \times 10^4$ )	1.38E-21	31.0	4.7
	PSI3.7 ( $2.55 \times 10^4$ )	1.84E-21	40.6	7.3

solution under the same buffer condition, 4.7%. We note that our model for the calculation here is a monomodal approximation and the accuracy of this approximation is improved by the distribution of smaller droplet size, since it is closer to a monomodal distribution. We believe that this is a very definitive experiment to show the droplet-induced effect.

These two examples clearly illustrate that care should be taken in interpreting the results of oligomer distributions measured from an ES source regardless of the analytical tool used (e.g., DMA or MS).

#### 4.2. Intrinsic Dimer Determination (Irreversible/Reversible, Total Concentration Known): Oligomerization of Rmab

In this section, we show a strategy to determine the concentration of intrinsic aggregates with the total concentration known. We also compare our results with the analytical ultracentrifuge (Ebel 2004; Howlett et al. 2006) measurements.

If we assume that only monomers and dimers are in solution and no higher aggregates and the total concentration  $C_p$  is

known, an additional relationship can be obtained:

$$C_p = C_{p1} + 2C_{p2}. \quad [36]$$

The ratio of intrinsic dimer to monomer of Rmab,  $C_{p2}/C_{p1}$ , can be obtained from Equations (27) and (36).

Using the data in Section 4.1.1, Table 2 shows the ratios of observed dimers to monomers for Rituxan at pH 7 measured in ES-DMA experiments at concentrations of 5, 10, 25, 50, and 100  $\mu\text{g/mL}$  and the intrinsic ratios at the same concentrations calculated based on Equations (27) and (36).

The results in Table 2 demonstrate that the actual dimer concentration in solution can be considerably smaller than that measured using an ES source, particularly at high concentration. For example at 100  $\mu\text{g/mL}$ , the observed dimer to monomer ratio was  $\sim 37\%$ , while after correction, the intrinsic ratio is 7.8%. At this high concentration, we were also able to compare with the analytical ultracentrifuge (Ebel 2004; Howlett et al. 2006) measurements directly on the solution, under the same conditions, which showed good agreement with our corrected value. We think the corrected value is even lower than 7.8%

TABLE 2

The ratios of observed dimers to monomers at pH 7 from DMA measurement, the ratios of intrinsic dimers to monomers calculated based on Equations (27) and (36), and the ratio of dimers to monomers measured by analytical ultracentrifuge for Rmab

	ES-DMA observed dimer to monomer ratio (%)	Intrinsic dimer to monomer ratio after correction for drop-induced dimers (%)	Analytical ultracentrifuge measured dimer to monomer ratio (%)
5 $\mu\text{g/mL}$	1.7	0	NA*
10 $\mu\text{g/mL}$	3.5	0.1	NA*
25 $\mu\text{g/mL}$	8.8	0.4	NA*
50 $\mu\text{g/mL}$	18.5	2.1	NA*
100 $\mu\text{g/mL}$	37.4	7.8	4.7

\*NA: not available; the sensitivity is below the detection limit.

if we use the general relationship, Equation (25), instead of the monomodal approximation relationship, Equation (27). The accuracy of monomodal approximation can be improved by using a smaller droplet size from ES since the distribution of smaller droplet sizes is closer to monodispersed distribution.

### 4.3. Intrinsic Dimer Determination (Irreversible Aggregation): Au-NPs

In this section, we discuss the implementation of an experimental strategy for irreversible aggregation, based on Equation (27) or (30), in which we determine the intrinsic aggregate concentration, without *a priori* knowledge of the drop size distribution. This basic strategy is to obtain the ratio of intrinsic dimer to monomer by a series of measurements at various dilutions.

For the electro spraying of Au-NPs in 2 mmol/L ammonium acetate buffer, the ES droplet follows a bimodal size distribution (Figure 2b). Equation (30) is used here for the calculation.

On the basis of Equation (30), assuming the intrinsic dimers of Au-NPs in solution are nonreversible, after a 2× dilution, an additional relationship can be obtained:

$$\frac{N_{o2,2x}}{N_{o1,2x}} = \frac{\bar{V}_{d2}C_{p1}/2}{2} + \frac{C_{p2}/2}{C_{p1}/2} = \frac{\bar{V}_{d2}C_{p1}}{4} + \frac{C_{p2}}{C_{p1}}, \quad [37]$$

where  $N_{o1,2x}$  is the observed number of monomers after 2× dilution and  $N_{o2,2x}$  is the observed number of dimers after 2× dilution.

Combining Equations (30) and (37), the ratio of intrinsic dimer to monomer of Au-NPs is

$$\frac{C_{p2}}{C_{p1}} = 2 \frac{N_{o2,2x}}{N_{o1,2x}} - \frac{N_{o2}}{N_{o1}}. \quad [38]$$

Figure 7 shows the observed size distribution at 2×, 4×, and 8× dilutions for 10 nm Au-NPs (Sample 1). The DMA voltage was scanned to detect particles up to 20 nm to enable the measurement of trimers that could be observed for the 2× dilution, but not for more dilute samples.

Table 3 shows the ratios of dimer to monomer measured with ES-DMA at 2×, 4×, and 8× dilutions of Au-NPs (Samples 1–4). A large proportion of oligomers are observed in these measurements. Using the theory described above, we now determine the true oligomer concentration.

For each sample, the ratio of intrinsic dimer to monomer is calculated based on Equation (38), using the ratio of 2× and 4× dilution and 4× and 8× dilution. Given the instability of the ES cone jet at low ionic strength and the propensity of the highly concentrated Au-NPs to aggregate, the intrinsic ratios calculated using 2× and 4× dilution and 4× and 8× dilution are mostly consistent. We note that with the dilution approach, it is not necessary to know the droplet size.

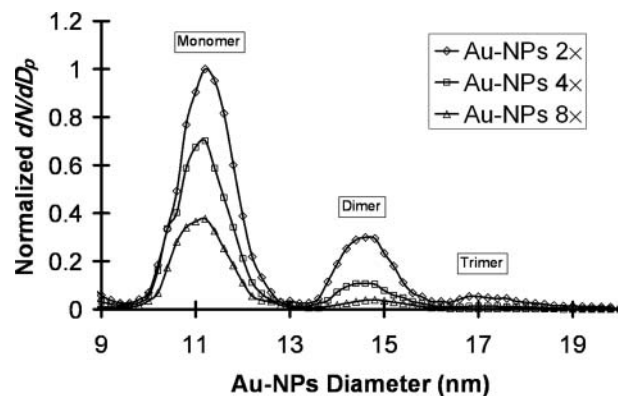


FIG. 7. ES-DMA size distributions of 10 nm Au-NPs, Sample 1. The rhombus, square, and triangle data markers are those of 2×, 4×, and 8× dilutions of the original sample, respectively. Each of the discernible oligomer peaks is labeled respectively.

### 4.4. Reversible Oligomerization: Relationship between Real Equilibrium Constant, $K$ , and Apparent Equilibrium Constant, $K_{app}$

If the intrinsic dimers in solution are fully reversible, the number concentrations of the intrinsic monomers and dimers are connected by an equilibrium constant  $K$ .

$$\frac{C_{p2}}{(C_{p1})^2} = K, \quad [39]$$

where  $C_{p1}$  is the number concentration of monomers in solution (particle number per unit volume) and  $C_{p2}$  is the number concentration of dimers in solution (particle number per unit volume).

From Equations (27) and (39), we get

$$\frac{N_{o2}}{N_{o1}} = \left( \frac{\bar{V}_d}{2} + K \right) C_{p1}. \quad [40]$$

If not considering droplet-induced aggregation, the apparent equilibrium constant,  $K_{app}$ , is defined by the observed monomer concentration  $C_{o1}$  and the observed dimer concentration  $C_{o2}$  by  $K_{app} = \frac{C_{o2}}{(C_{o1})^2}$ . We can obtain

$$\frac{N_{o2}}{N_{o1}} = \frac{C_{o2}}{C_{o1}} = K_{app}C_{o1}. \quad [41]$$

By comparing Equation (40) with Equation (41), the real equilibrium constant  $K$  can be obtained:

$$K = \frac{C_{o1}}{C_{p1}} K_{app} - \frac{\bar{V}_d}{2}, \quad [42]$$

where  $C_{p1}$  is the number concentration of monomers in solution and  $C_{o1}$  is the observed number concentration of monomers after ES.

TABLE 3

The ratios of observed dimers to monomers from DMA measurement, and the ratios of intrinsic dimers to monomers calculated based on Equation (38) for 10 nm Au-NPs

	ES-DMA observed dimer to monomer ratio (%)			True dimer to monomer ratio (i.e., after droplet-induced effects removed) (%)	
	2×	4×	8×	Based on 2× and 4×	Based on 4× and 8×
Sample 1	31.3	17.3	11.5	3.3	5.7
Sample 2	33.2	18.1	12.3	3.0	6.5
Sample 3	36.3	19.5	11.1	2.7	2.7
Sample 4	35.7	19.4	12.1	3.1	4.8

Since  $C_{o1}$  is less than  $C_{p1}$  because of the induced dimer formation, we can see that the apparent equilibrium constant  $K_{app}$ , when the induced aggregation is not considered, is higher than the true value, and the difference is more than half of the droplet volume  $\bar{V}_d/2$ .

Using the relationships above, we discuss the results from an ES-MS (without a neutralizer) study by Nettleton et al. (2000) to characterize the oligomers of insulin. Nettleton et al. (2000) plotted the fraction of dimer observed by MS against the insulin concentration from 2 to 200  $\mu\text{mol/L}$  at pH 3.3 and 22°C (Figure 8, rhombuses). The fraction of dimer was defined as the ratio of summation of the peaks assigned to the dimer to the total signal intensity. In this insulin concentration range, only monomer and dimer peaks were observed by MS, so the fraction of dimer is equal to the number of observed dimers divided by the total number of observed dimers and monomers. Nettleton et al. used the plot to obtain the apparent equilibrium constant  $K_{app}$ .

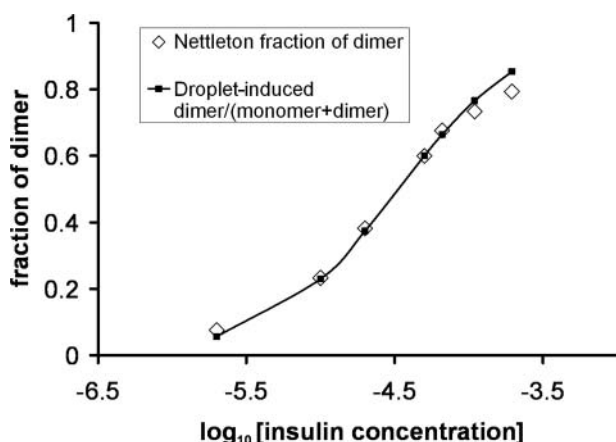


FIG. 8. The fraction of insulin dimer versus insulin total in the concentration range of 2–200  $\mu\text{mol/L}$  at pH 3.3 and 22°C (rhombuses) as measured by Nettleton et al. (2000) using nano-ES/MS (line with open diamonds). The ratio of dimer/(monomer + dimer) calculated by Equation (43) using the droplet-induced dimer for the concentration range of 2–200  $\mu\text{mol/L}$  (line with filled squares).

On the basis of the droplet-induced aggregation of identical particles following Equation (5), the fraction of induced dimer is

$$\frac{N_{o2}}{N_{o1} + N_{o2}} = \frac{P(2, \bar{\lambda})}{P(1, \bar{\lambda}) + P(2, \bar{\lambda})} = \frac{\bar{\lambda}}{2 + \bar{\lambda}} = \frac{C_{p1} \bar{V}_d^*}{2 + C_{p1} \bar{V}_d^*}, \quad [43]$$

where  $\bar{V}_d^*$  is the average droplet volume, if the observed dimers are all droplet induced, and  $C_{p1}$  is the insulin number concentration under this situation.

We can estimate the average droplet volume,  $\bar{V}_d^*$ , by using the protein concentration and the ratio of dimer to the total oligomer (Equation (43)). The fourth point in Nettleton's plot is then given by  $\log_{10}[C_p] = -4.3$  and the fraction of dimer = 0.6. This value is used to estimate the average droplet volume as ca.  $\bar{V}_d^* = 9.94 \times 10^{-23} \text{ m}^3$ . We then use this average droplet volume to calculate the fraction of dimer at other concentrations in Nettleton's plot based on Equation (43) and obtain the second curve in Figure 8 (line with filled squares). The curve deduced from the droplet-induced model essentially superimposes on Nettleton's data and is highly suggestive that an alternative explanation to Nettleton's plot is that the droplet-induced aggregation is responsible for most of the dimers seen.

Given that for the Nettleton's data, we do not measure the droplet volume, our discussion necessarily assumes that the ES process of insulin is governed by the droplet-induced aggregation mechanism resulting from the CRM, rather than any ion emission mechanism. However, as long as the fraction of insulin particles generated by the droplet-induced aggregation mechanism is a fixed value in the insulin concentration range from 2 to 200  $\mu\text{mol/L}$ , the discussion above is still valid. This is then an alternative explanation of Nettleton's plot (Nettleton et al. 2000).

## 5. SUMMARY OF CASES AND FORMULAS

In this section, each limiting case and the relevant formula is listed.

Definitions:

$f(D_d)$  = the droplet size distribution, which can be measured experimentally from sucrose solution under the same buffer condition (Section 3.4)

$D_d$  = the droplet diameter,  
 $\bar{V}_d$  = the average droplet volume as determined from  $f(D_d)$ ,  
 $N_{o1}$  = the observed number of monomers after ES,  
 $N_{o2}$  = the observed number of dimers after ES,  
 $C_{p1}$  = the number concentration of monomers in the original solution,  
 $C_{p2}$  = the number concentration of dimers in the original solution.

### 5.1. Intrinsic Dimer Determination (Irreversible/Reversible; Total Concentration Known; Monomodal and Narrow Droplet Size Distribution $f(D_d)$ ):

- Only monomers and dimers are in solution, i.e., no higher aggregates.
- Total concentration of the analyte in solution,  $C_p$ , is known.

The ratio of intrinsic (in solution) dimer to monomer concentration,  $C_{p2}/C_{p1}$ , can be obtained from Equations (27) and (36).

$$C_p = C_{p1} + 2C_{p2}, \quad [36]$$

$$\frac{N_{o2}}{N_{o1}} \approx \frac{P_2|_{V_d=\bar{V}_d}}{P_1|_{V_d=\bar{V}_d}} = \frac{\bar{V}_d C_{p1}}{2} + \frac{C_{p2}}{C_{p1}}. \quad [27]$$

### 5.2. Intrinsic Dimer Determination (Irreversible/Reversible; Total Concentration Known; Bimodal Droplet Size Distribution $f(D_d)$ ):

- Size distribution  $f(D_d)$  is bimodal.
- $\bar{V}_{d2}(C_{p1} + C_{p2}) \leq 1$ .

The ratio of intrinsic dimer to monomer,  $C_{p2}/C_{p1}$ , can be obtained from Equations (30) and (36).

$$C_p = C_{p1} + 2C_{p2}, \quad [36]$$

$$\frac{N_{o2}}{N_{o1}} \approx \frac{\bar{V}_{d2} C_{p1}}{2} + \frac{C_{p2}}{C_{p1}}, \quad [30]$$

where  $\bar{V}_{d2}$  is the average droplet volume within range 2 (Figure 2b).

### 5.3. Intrinsic Dimer Determination (Irreversible Aggregation)

The ratio of intrinsic dimer to monomer for irreversible aggregation,  $C_{p2}/C_{p1}$ , is

$$\frac{C_{p2}}{C_{p1}} = 2 \frac{N_{o2,2x}}{N_{o1,2x}} - \frac{N_{o2}}{N_{o1}}, \quad [38]$$

where  $N_{o1,2x}$  is the observed number of monomers after  $2x$  dilution and  $N_{o2,2x}$  is the observed number of dimers after  $2x$  dilution.

## 6. CONCLUSIONS

Electrospray (ES) sampling is widely used to introduce non-volatile material into the gas phase for characterization by MS or ion mobility. In using an ES sampling process for characterizing protein or nanoparticle aggregation, one must carefully evaluate if the aggregates observed are intrinsic to the solution or induced by the ES process. We have developed a statistical model to calculate the intrinsic oligomer ratios in solution from the experimentally determined distributions by considering the droplet size distribution and physical-induced aggregation in ESs. Using this approach, we show that the extent of droplet-induced aggregation can be severe. We demonstrate that the droplet-induced aggregation can bias data obtained by ES-MS and the data obtained by ES-MS or ES-DMA need to be carefully scrutinized to avoid erroneous interpretation. On the basis of our experimentally validated model, a quantitative distribution of intrinsic particle aggregation in ES can be obtained.

## REFERENCES

- Abate, A. R., Chen, C. H., Agresti, J. J., and Weitz, D. A. (2009). Beating Poisson Encapsulation Statistics Using Close-Packing Ordering. *Lab Chip*, 9:2628–2631.
- Ayed, A., Krutchinsky, A. N., Ens, W., Standing, K. G., and Duckworth, H. W. (1998). Quantitative Evaluation of Protein-Protein and Ligand-Protein Equilibria of a Large Allosteric Enzyme by Electrospray Ionization Time-of-flight Mass Spectrometry. *Rapid Commun. Mass Spectrom.* 12:339–344.
- Bacher, G., Szymanski, W. W., Kaufman, S. L., Zöllner, P., Blaas, D., and Allmaier, G. (2001). Charge-Reduced Nano Electrospray Ionization Combined with Differential Mobility Analysis of Peptides, Proteins, Glycoproteins, Noncovalent Protein Complexes and Viruses. *J. Mass Spectrom.* 36:1038–1052.
- Chen, D.-R., Pui, D. Y. H., and Kaufman, S. L. (1995). Electro spraying of Conducting Liquids for Monodisperse Aerosol Generation in the 4 nm to 1.8  $\mu\text{m}$  Diameter Range. *J. Aerosol Sci.* 6:963–977.
- Dole, M., Mack, L. L., and Hines, R. L. (1968). Molecular Beams of Macroions. *J. Chem. Phys.* 49:2240–2249.
- Ebel, C. (2004). Analytical Ultracentrifugation for the Study of Biological Macromolecules. *Prog. Colloid Polym. Sci.* 127:73–82.
- Edd, J. F., Carlo, D. D., Humphry, K. J., Köster, S., Irimia, D., Weitz, D. A., and Toner, M. (2008). Controlled Encapsulation of Single-Cells into Monodisperse Picolitre Drops. *Lab Chip* 8:1262–1264.
- Fernandez de la Mora, J. (2000). Electrospray Ionization of Large Multiply Charged Species Proceeds Via Dole's Charged Residue Mechanism. *Anal. Chim. Acta* 406:93–104.
- Gamero-Castano, M., and Fernandez de la Mora, J. (2000a). Kinetics of Small Ion Evaporation from the Charge and Mass Distribution of Multiply Charged Clusters in Electro sprays. *J. Mass Spectrom.* 35:790–803.
- Gamero-Castano, M., and Fernandez de la Mora, J. (2000b). Mechanisms of Electrospray Ionization of Singly and Multiply Charged Salt Clusters. *Anal. Chim. Acta* 406:67–91.
- Gaskell, S. J. (1997). Electrospray: Principles and Practice. *J. Mass Spectrom.* 32:677–688.
- Hogan, C. J., and Biswas, P. (2008a). Monte Carlo Simulation of Macromolecular Ionization by Nanoelectrospray. *J. Am. Soc. Mass Spectrom.* 19:1098–1107.
- Hogan, C. J., and Biswas, P. (2008b). Porous Film Deposition by Electrohydrodynamic Atomization of Nanoparticle Sols. *Aerosol Sci. Tech.* 42:75–85.
- Hogan, C. J., Carroll, J. A., Rohrs, H. W., Biswas, P., and Gross, M. L. (2009). Combined Charged Residue-Field Emission Model of Macromolecular Electrospray Ionization. *Anal. Chem.* 81:369–377.

- Howlett, G. J., Minton, A. P., and Rivas, G. (2006). Analytical Ultracentrifugation for the Study of Protein Association and Assembly. *Curr. Opin. Chem. Biol.* 10:430–436.
- Iribarne, J. V., and Thomson, B. A. (1976). On the Evaporation of Small Ions from Charged Droplets. *J. Chem. Phys.* 64:2287–2294.
- Kaufman, S. L. (2000). Electrospray Diagnostics Performed by Using Sucrose and Proteins in the Gas-Phase Electrophoretic Mobility Molecular Analyzer (GEMMA). *Anal. Chim. Acta* 406:3–10.
- Kaufman, S. L., Skogen, J. W., Dorman, F. D., and Zarrin, F. (1996). Macromolecule Analysis Based on Electrophoretic Mobility in Air: Globular Proteins. *Anal. Chem.* 68:1895–1904.
- Kearle, P. (2000). A Brief Overview of the Present Status of the Mechanisms Involved in Electrospray Mass Spectrometry. *J. Mass Spectrom.* 35:804–817.
- Kearle, P., and Tang, L. (1993). From Ions in Solution to Ions in the Gas Phase: The Mechanism of Electrospray Mass Spectrometry. *Anal. Chem.* 65:972–986.
- Kim, S. H., and Zachariah, M. R. (2005). In-Flight Size Classification of Carbon Nanotubes by Gas Phase Electrophoresis. *Nanotechnology* 16:2149–2152.
- Kim, S. H., and Zachariah, M. R. (2006). In-Flight Kinetic Measurements of the Aerosol Growth of Carbon Nanotubes by Electrical Mobility Classification. *J. Phys. Chem. B* 110:4555–4562.
- Kim, S. H., and Zachariah, M. R. (2007). Gas-Phase Growth of Diameter-Controlled Carbon Nanotubes. *Mater. Lett.* 61:2079–2083.
- Ku, B. K., and Fernandez de la Mora, J. (2004). Cluster Ion Formation in Electrosprays of Acetonitrile Seeded with Ionic Liquids. *J. Phys. Chem. B* 108:14915–14923.
- Lane, L. A., Ruotolo, B. T., Robinson, C. V., Favrin, G., and Benesch, J. L. P. (2009). A Monte Carlo Approach for Assessing the Specificity of Protein Oligomers Observed in Nano-Electrospray Mass Spectra. *Int. J. Mass Spectrom.* 283:169–177.
- Lenggoro, I. W., Xia, B., and Okuyama, K. (2002). Sizing of Colloidal Nanoparticles by Electrospray and Differential Mobility Analyzer Methods. *Langmuir* 18:4584–4591.
- Lewis, K. C., Dohmeier, D. M., and Jorgenson, J. W. (1994). Electrospray-Condensation Particle Counter: A Molecule-Counting LC Detector for Macromolecules. *Anal. Chem.* 66:2285–2292.
- Light-Wahl, K. J., Schwartz, B. L., and Smith, R. D. (1994). Observation of the Noncovalent Quaternary Associations of Proteins by Electrospray Ionization Mass Spectrometry. *J. Am. Chem. Soc.* 116:5271–5278.
- Light-Wahl, K. J., Winger, B. E., and Smith, R. D. (1993). Observation of the Multimeric Forms of Concanavalin A by Electrospray Ionization Mass Spectrometry. *J. Am. Chem. Soc.* 115:5869–5870.
- Nettleton, E. J., Paula Tito, M. S., Bouchard, M., Dobson, C. M., and Robinson, C. V. (2000). Characterization of the Oligomeric States of Insulin in Self-Assembly and Amyloid Fibril Formation by Mass Spectrometry. *Biophys. J.* 79:1053–1065.
- Pease, L. F., Elliott, J. T., Tsai, D.-H., Zachariah, M. R., and Tarlov, M. J. (2008). Determination of Protein Aggregation with Differential Mobility Analysis: Application to IgG Antibody. *Biotechnol. Bioeng.* 101:1214–1222.
- Tsai, D.-H., Zangmeister, R. A., Pease, L. F., III, Tarlov, M. J., and Zachariah, M. R. (2008). Gas-Phase Ion-Mobility Characterization of SAM-Functionalized Au Nanoparticles. *Langmuir* 24:8483–8490.
- Wiedensohler, A. (1988). Technical Note: An Approximation of the Bipolar Charge Distribution for Particles in the Submicron Range. *J. Aerosol Sci.* 19:387–389.